JTTEE5 8:117-124

Oxidation and Particle Deposition Modeling in Plasma Spraying of Ti-6Al-4V/SiC Fiber Composites

E. Cochelin, F. Borit, G. Frot, M. Jeandin, L. Decker, D. Jeulin, B. Altaweel, V. Michaud, and P. Noël

(Submitted 19 May 1998; in revised form 22 October 1998)

Plasma spraying is known to be a promising process for the manufacturing of Ti/SiC long-fiber composites. However, some improvements remain for this process to be applied in an industrial route. These include: oxygen contamination of the sprayed material through that of titanium particles before and during spraying, damage to fibers due to a high level of thermal stresses induced at the spraying stage, adequate deposition of titanium-base powder to achieve a low-porosity matrix and good impregnation of the fiber array. This article deals with work that resulted in a threefold study of the process. Oxidation was studied using electron microprobe analysis of elementary particles quenched and trapped into a closed box at various given flight distances. Oxygen diffusion phenomena within the particles are discussed from a preliminary theoretical approach coupled with experimental data. Isothermal and thermomechanical calculations were made using the ABAQUS code to determine stresses arising from contact of a liquid Ti-6Al-4V particle onto a SiC fiber. On the scale of the sprayed powder flow, a two-dimensional new type of model simulating the deposition of droplets onto a substrate was developed. This new type of model is based on a lattice-gas automaton that reproduces the hydrodynamical behavior of fluids.

Keywords composite, lattice-gas, LGM, modeling, oxidation, plasma spraying, SiC fiber, Ti-6Al-4V, TMC

1. Introduction

Since the pioneering work from the General Electric Company in the early 1980s (Ref 1, 2) titanium-matrix composites (TMCs), primarily Ti-6Al-4V with SiC long fibers, have shown promise to improve gas turbine aeroengines. These would, for example, allow at the compressor stage for an upgrade from the conventional disk and dovetail blade arrangement to the much more efficient and lighter (up to a 70% weight reduction) "bling," that is, TMC blade ring. Several other aircraft applications of TMCs, although less striking, are reported, for example, struts and actuators.

Most TMC manufacturing routes involve two steps, the layup of a "green" TMC preform of properly placed fibers and matrix and the subsequent consolidation by hot pressing. Numerous studies were devoted to the various routes and materials properties (e.g., Ref 3). Apart from the conventional solid-state stacking of alternate titanium-base foil SiC fiber layers, two main processes are currently developed: deposition from the vapor phase (by sputtering for example) and plasma spraying of the titanium matrix onto the fibers. Compared to the route using evaporated titanium-coated fibers, plasma spraying appears to be more flexible and efficient because any matrix composition can be obtained in a fairly rapid manufacturing step of TMC monotapes.

Improvements, however, can be made in promoting plasma spraying for an industrial route. These should result in high cleanliness of the composite, minimum fiber damage, and reliable fiber spacing. This article addresses these major points.

The first part of this article deals with oxygen contamination of the sprayed material mainly through microanalysis of sprayed particles. The contamination problem has received little attention because it is often assumed that chemical contamination can be controlled and limited by vacuum plasma spraying (i.e., more precisely spraying under a low pressure) (Ref 4). However, due to the very high reactivity of titanium, very low contents of oxygen in the surrounding atmosphere might be sufficient to impair the material soundness.

The second aspect of this article concerns an approach to fiber damage through thermomechanical modeling of stresses within a SiC fiber when in contact with a liquid Ti-6Al-4V droplet. Fiber damage is all the more important to study because direct current (dc) systems for plasma spraying are envisaged rather than radiofrequency (rf) systems that were initially used for TMCs (Ref 1, 2). The latter were proposed to be less detrimental mechanically due to lower impact velocities (Ref 5).

The third part of this article presents the use of a new type of modeling, lattice-gas modeling (LGM), of matrix buildup through droplet deposition. There is a strong demand for modeling to improve TMC properties for commercial exploitation. The level of residual porosity, which is currently unacceptable,

E. Cochelin, F. Borit, G. Frot, and **M. Jeandin,** Ecole des Mines de Paris/C2P, Center for Plasma Processing, BP 87, 91003 Evry Cedex, France; **L. Decker** and **D. Jeulin,** Ecole des Mines de Paris/Centre de Morphologie Mathématique, 35, rue Saint Honoré, 77305 Fontainebleau, France; **B. Al Taweel** and **V. Michaud,** Ecole Centrale de Paris/MSSMAT, Grande Voie des Vignes, 92295 Châtenay-Malabry Cedex, France; and **P. Noël,** MATRA-BAe Dynamics, 20-22, Grange Dame Rose, BP 150, 78141 Vélizy Cedex, France. Contact M. Jeandin at e-mail: jeandin@mat.cnsmp.fr.

typically around 20%, could be reduced by changing the processing parameters including torch/powder flow incidence angle, trajectories, interfiber spacings, particle size, as shown recently by Clyne et al. (Ref 6). However, no flexible or powerful modeling tool is available to optimize the main influencing parameters. Lattice-gas modeling was developed to contribute to meeting these requirements.

2. Materials and Processes

Ti-6Al-4V T-1149 powder from CERAC (Milwaukee, WI) with a size of 70 to 120 μm was used. The powder chemical composition (Table 1) shows a nominal oxygen content lower than 0.12%.

Powder was vacuum plasma sprayed (VPS) using industrial facilities that were especially modified by Matra-BAe Dynamics (Vélizy, France) for processing in a high-purity atmosphere. Additional spraying experiments for the modeling part of the study were carried out using the Sulzer-Metco CAPS (Controlled Atmosphere Plasma Spraying) unit of the Center for Plasma Processing (C2P, Evry, France). The versatility and flexibility of the CAPS system was exploited to extend the range of operating spray conditions (e.g., under pressure) to modify the sprayed microstructures (Ref 7). Other materials and processes specific to a given part of this study are described in the corresponding section.

Table 1 Chemical composition of Ti-6Al-4V powder

	Composition, wt%			
Powder	**Ti**	**Al**	**V**	**O**
Ti-6Al-4V	90.0	6.0	4.0	<0.12

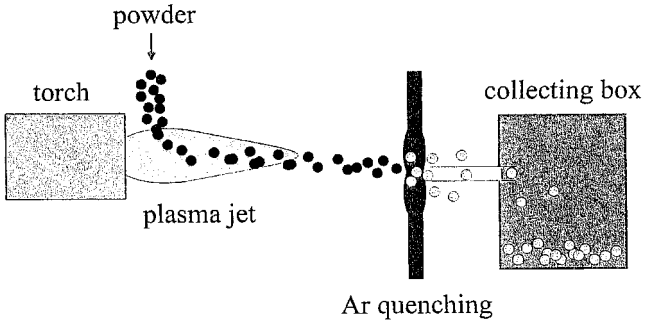

Fig. 1 Experimental setup for collecting droplets

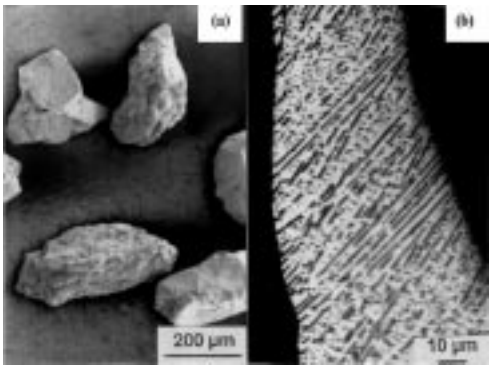

Fig. 2 Scanning electron micrograph (a) and cross-section optical (b) images of loose Ti-6Al-4V powder

3. Oxidation of Ti-6Al-4V Powders

The oxidation study was based on the determination of oxygen distribution within particles collected in the spray cone. Electron probe microanalysis (EPMA) of droplets quenched at various distances from the gun nozzle exit was used.

3.1 Spray Experiments

The most common procedures for investigation of the progression of particle melting and structure are the so-called WIPE (Ref 8) and more recently, LINESCAN (Ref 9) tests. For this study, a special setup was developed to collect droplets at distances, that is, 80, 100, 120, 140, 160, and 180 mm from the gun nozzle exit.

The setup (Fig. 1) consisted of a stainless steel tube 4 mm in diameter along the plasma jet axis. Some droplets passed through the tube orifice and were caught. Just before reaching the aperture, the droplets were quenched with argon gas cooling. Once in the tube, the solid particles from droplets were then kept in a closed box welded to the tube. The efficiency of this collecting process was estimated to be no more than a few percent, which was, however, enough to obtain significant sampling of the droplet flow.

3.2 Electron Probe Microanalysis

Electron probe microanalysis was applied to loose powders. Additional observations used conventional optical microscopy and high-resolution scanning electron microscope (field-effect LEO 982 SEM; LEO Elektronenmikroskopie GmbH, Oberkochen, Germany).

The starting batch of powder (Table 1) was made of crushed, angular particles with an oxygen content of less than 1200 ppm (Fig. 2a). The particles exhibited a conventional $\alpha + \beta$ microstructure (Fig. 2b), which could be observed after etching (10 vol% HF, 5 vol% HNO_3, and 85 vol% H_2O).

Sample Preparation. Careful preparation of the EPMA samples was necessary to obtain the most significant results, especially near the particle surface where some oxygen evolution was expected. This evolution was assumed to result from oxidation/deoxidation and/or oxygen diffusion prior to and during spraying.

Ti-6Al-4V particles were mixed with chips of Wood's alloy (i.e., low melting temperature, 72 °C, 50Bi-25Pb-12.5Sn-12.5Cd alloy) and heated to form coated particles due to melting of the Wood's alloy. These were then embedded using uniaxial pressing (180 °C, 20 kN) in a diphthalate resin reinforced with glass fibers. Using a conventional organic resin for direct embedding of the particles would not have been suitable due to the presence of oxygen in the resin, which would have prevented oxygen analysis near the particle surface.

Analysis Procedure. A CAMECA SX50 microprobe (CAMECA, Courbevoie, France) was used for the EPMA. As required for accurate results, the analyses were applied to unetched mirrorlike polished particle cross sections. Composition profiles for the main elements, primarily oxygen, were

determined from the core to the surface of the particles. Spot analyses were applied by stepping 1 μm. The use of a shorter step would not have been realistic because the spatial resolution for an elementary analysis could not be better than 1 μm due to a minimum electron/matter interaction volume, which corresponds to about 1 μm^3, whatever the analysis conditions.

Bismuth exists in the Wood's alloy but not in the titanium-base particles, and therefore it was chosen as an element to define accurately the location of the particle surface during profile analysis.

For several particle cross sections, two composition line profiles were measured. Because the results were quite similar for the two sample/spectrometer orientations, all the profiles were ascertained to be valid, provided there was no influence of sample preparation.

Confocal microscopy was applied to the zones used for EPMA profiles in order to obtain the height profile at the sample surface corresponding exactly to a given EPMA profile (Fig. 3), the latter being revealed by beam-contamination tracing.

The profiles determined for several particles (e.g., that of Fig. 4) indicate that there was no influence of the slight surface roughness due to polishing. Only a very smooth height decrease with a very low (less than 1 μm in height) step at the particle-Wood's alloy embedding interface could be detected. This did not result in changes in the corresponding composition profile because no correlation could be established between height and EPMA profiles.

EPMA Results and Discussion. Some particles spheroidized in the plasma flame depended on dwell time in hot zones, and therefore on flight distance before quenching at the trap box. However, no relationship between the number of spheroidized particles and the distance to the box could be established in this work. Further particle-catching tests should be carried out and duplicated to obtain a more numerous sampling of particles. This would allow examination of the influence of the box aperture location and fix it accurately.

More than 25 series of complete EPMA profiles were determined for particle samples of different (i.e., from angular to purely spherical) shapes for different distances. This article shows a limited number of results and profiles that are, however, typical of the experiments.

The reference microstructural chemical state, that is, that of particles in the starting powder batch, was characterized by a quasi-constant oxygen level of 2.6 to 2.7 wt%, and typical variations of aluminum and vanadium around 6 and 4 wt%, respectively. These variations resulted from the spot analysis procedure applied to the two-phase α-β microstructure (α, rich in aluminum; β, rich in vanadium).

When processed in the plasma jet, particles underwent chemical homogenization that could be of two types. The first consisted of solid-state (on the particle scale) homogenization, which left the shape of the starting particle unchanged, that is, angular (Fig. 5). The second was liquid-phase homogenization, which was coupled with particle spheroidization (Fig. 6).

Solid-state homogenization resulted in smoothing of the aluminum, vanadium, and oxygen profiles with reduced variations around an average level of respectively 6, 4, and 3 wt% (Fig. 5).

Liquid-state homogenization resulted in flattening these same profiles in the core of the particle (Fig. 6). This corresponded to microstructural refinement due to quenching from the liquid alloy.

In addition, a significant increase of the oxygen content over about 10 μm typically at the surface of the particle was shown, coupled with a vanadium decrease over the same depth (the aluminum content remaining constant). This gradient could be attributed to diffusion of oxygen from the spraying atmosphere. It can be assumed that there was no significant contribution to the

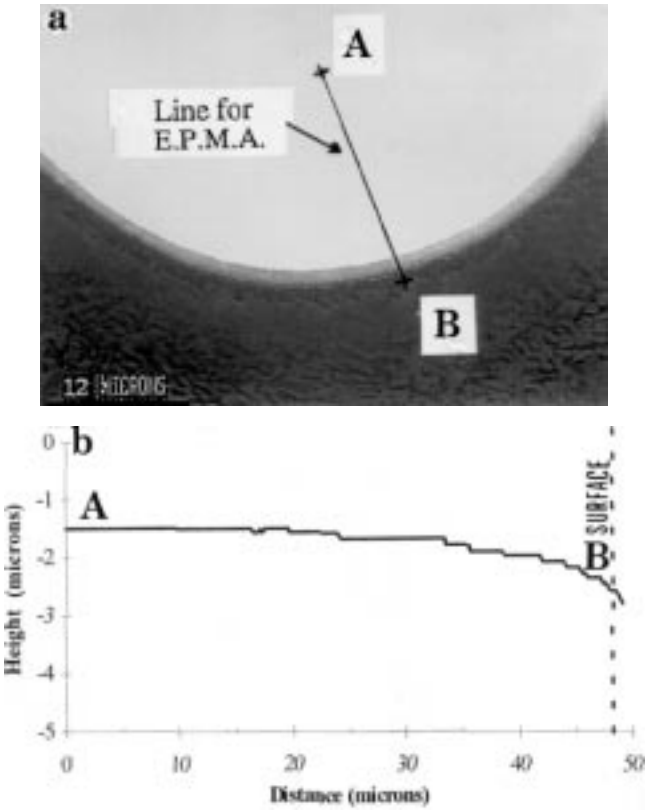

Fig. 3 (a) Topographic confocal image of a particle exhibiting the beam pass for EPMA (see Fig. 6). (b) Corresponding height profile.

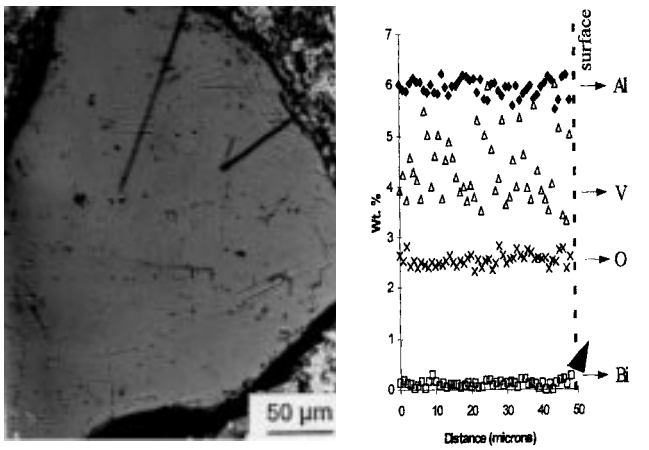

Fig. 4 Electron probe microanalysis of reference Ti-6Al-4V

gradient from dissolution of superficial oxides at the surface prior to spraying because no oxygen (on the analysis scale, which was consistent with the amount required for a significant contribution) was detected at the reference powder surface.

The oxygen (and vanadium) gradient was related to a microstructure characterized by a rather coarse β phase in an oxygen-rich rim surrounding an α + β finely structured core (Fig. 7).

The study of the EPMA profiles indicated that both types of homogenization processes were promoted when increasing the nozzle-box distance/dwelling. Further samples of particles should be studied with analyses involving particle size and the initial microstructural fineness, in addition to the particle shape. This would be needed to prevent cross-section effects related to the interpretation of three-dimensional phenomena from two-dimensional data and the influence of microstructural heterogeneity between particles of a given powder sample.

From the conventional one-dimensional expression of the diffusion law:

$$C(x,t) = C_O\left(1 - \text{erf}\,\frac{x}{2\sqrt{D\,(T)\cdot t}}\right) + D_O$$

where $C(x,t)$ is the oxygen content at a distance x, in wt%; $D\,(T)$ is the diffusion coefficient, in cm^2/s; x is the distance, in cm; t, is the time, in s; T is the temperature; C_O and D_O are constants; and erf is error function. One can obtain, using simplifying assumptions for t and T due to nonequilibrium conditions at spraying:

$$C(x) = C_O\left(1 - \text{erf}\,\frac{x}{2\sqrt{\chi}}\right) + D_O$$

with χ as a constant (in cm^2).

The experimental oxygen profiles were used to fit this equation and the constants determined as: $C_O \approx 1.27$ wt%, $D_O \approx 2.92$ wt%, and $\chi \approx 8.8 \times 10^{-8}\ cm^2$. The order of magnitude of the diffusion coefficient would be, therefore, less than $10^{-8}\ cm^2/s$. This ascertained a volume diffusion phenomenon, in contrast with intergranular diffusion, for which the diffusion coefficient would have been much higher (around $10^{-5}\ cm^2/s$, typically).

4. Fiber Damage Modeling

It has been observed that SiC fibers (SCS-6 from Avco-Textron, Lowell, MA, USA, and Sigma from B.P., Farnborough, UK) might exhibit a decrease of about 5% or more in their mean fracture stress when tested in tension after having been extracted from a preimpregnated sheet, in comparison to reference fibers (Ref 10). This drop in the fiber mechanical properties after plasma spraying may result from various causes. The fibers

Table 2 Computation conditions

		Thermomechanical	
Type	**Isothermal**	**g2000f20t2000**	**g2000f500**
Fiber initial temperature, °C	2000	20	500
Cooling conditions	Isothermal, to 20 °C	1°/μs for the metal	1°/μs, for the metal, then isothermal from 500
Boundary conditions	…	Adiabatic	Adiabatic

	Thermomechanical		
Type	**g2000f1000**	**g2000f20ext20**	**g2000f20t1000**
Fiber initial temperature, °C	1000	20	20
Cooling conditions	1°/μs, for the metal, then isothermal from 1000 °C	1°/μs for the metal up to 20 °C	2°/μs, for the metal up to 20 °C
Boundary conditions	Adiabatic	External temperature, 20 °C	Adiabatic

g, drop in temperature in °C; f, fiber temperature in °C; t, cooling time in microseconds; ext, imposed temperature on the external boundary of the fiber in °C

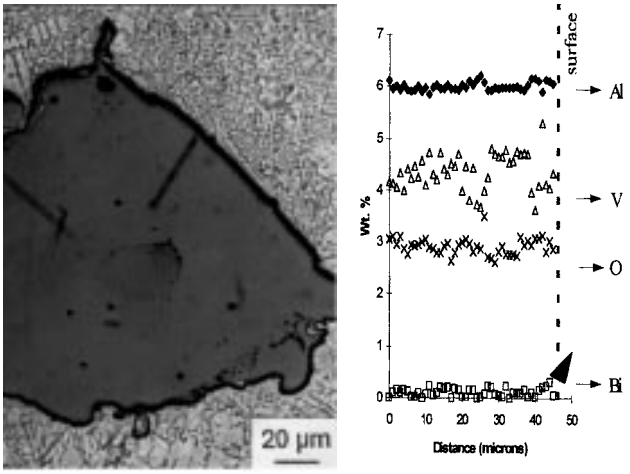

Fig. 5 Electron probe microanalysis of homogenized Ti-6Al-4V

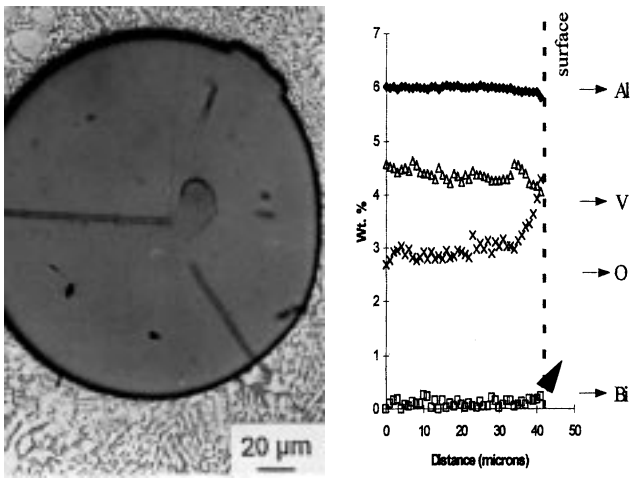

Fig. 6 Electron probe microanalysis of spheroidized Ti-6Al-4V

could be damaged during handling and while positioned around the mandrel. They could also experience stresses during plasma spraying where damage could be induced from: (1) the mechanical effect of the metal droplets impacting on the fibers at velocities on the order of 100 m/s; (2) rapid thermal exchange between molten droplets (at about 2000 °C) and the cold fiber, and (3) stresses developing during cool down due to the difference in coefficients of thermal expansion between SiC and titanium alloys.

Scanning electron microscopy observation of extracted SiC fibers did not reveal any visible defect on the fiber surface. However, as evaluated by Ochiai using linear elastic fracture mechanics (Ref 11), microcracks as small as 0.1 μm deep in a carbon fiber coating could lead to a twofold reduction in the fiber stress to fracture. It was, therefore, useful to identify the causes leading to fiber damage by numerical means, because experimental observation is often inconclusive.

In this part of the work, the contribution of stresses arising from thermal shock and cool down were evaluated using finite element analysis.

4.1 Assumptions and Conditions

The impact of the metal droplet was neglected, and it was assumed that spreading took place very rapidly before solidification occurred. This was already shown to be valid in typical plasma spraying conditions (Ref 12). A 2 μm thick layer of Ti-6Al-4V from a particle that was originally 50 μm in diameter was considered to be in contact with a cylindrical homogeneous fiber of 140 μm in diameter, (Fig. 8). Under typical plasma spraying conditions, the cooling rate is about 10^6 K/s, that is, 1 K per μs. A first evaluation of the timescale required to equilibrate the thermal gradients by conduction, $t = d^2/\alpha$, where d is the characteristic distance, and α is the thermal diffusivity of the material, yielded:

- For the SiC fiber, $d = 70$ μm, $\alpha = 5.39 \times 10^{-5}$ m^2/s, which gave $t \approx 90$ μs
- For Ti-6Al-4V metal, $d = 1$ μm, $\alpha = 2.77 \times 10^{-6}$ m^2/s, which gave $t \approx 0.25$ μs.

The metal could, therefore, be considered to have a uniform temperature. However, thermal gradients need to be considered in the fiber. A coupled thermomechanical computation was, therefore, necessary for a cooling rate above about 10^4 K.

Finite element computation was performed with ABAQUS (from HKS, Pawtucket, RI, USA) software, using two-dimensional plane-strain conditions and linear elements. The mesh (Fig. 8) was created using I-Deas Master Series (from SDRC, Milford, OH, USA). The constitutive behavior of Ti-6Al-4V was assumed to be elastoplastic and a function of temperature (with a negligible modulus above the melting point), and that of SiC was assumed to be linear elastic, isotropic (due to unavailability of data for the anisotropic properties of the fiber). Heat capacity, thermal conductivity, and coefficient of thermal expansion (CTE) were also assumed to vary with temperature. All relevant data were obtained from references (Ref 10, 13, 14). Thermal transfer at the nodes belonging to the fiber and the metal was assumed to be perfect. The interfacial temperature was the same in the fiber and in the metal.

Table 3 Stress characteristics

Name	σ_{11} max, MPa location, time	σ_{22} max, MPa location, time
Isotherme	**300, lim, end**	**298, lim, end**
2000f20t2000	1950, axe, 1 μs	939, lim, end
g2000f500	1612, axe, 1 μs	756, lim, end
g2000f1000	997, axe, 1.5 μs	585, lim, end
g2000f20ext20	1780, axe, 1.5 μs	897, lim, end
g2000f20t1000	1907, axe, 0.4 μs	942, lim, end

g, drop in temperature in °C; f, fiber temperature in °C; t, cooling time in microseconds; ext, imposed temperature on the external boundary of the fiber in °C

Fig. 7 Scanning electron micrograph of cross-section image of etched spheroidized Ti-6Al-4V. This same particle was used for analysis, the results of which are in Fig. 6 (analysis line in the lower part of the picture).

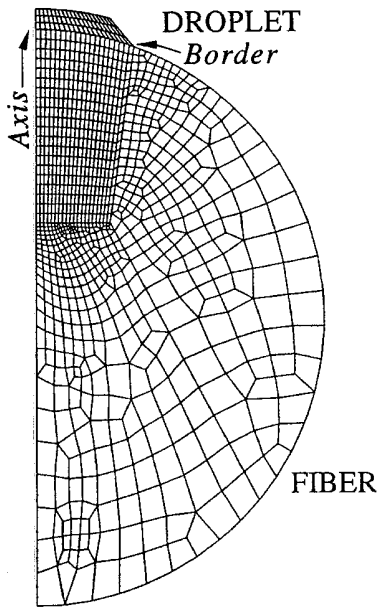

Fig. 8 Mesh used in FEM calculations (fiber of 140 μm in diameter)

Six types of computations were performed with different boundary or initial conditions (Table 2). The initial metal temperature was chosen to be 2000 °C in all cases. The first computation involved isothermal cooling from 2000 to 20 °C to evaluate the stresses created by CTE differences only, as might happen during slow cooling. The other computations involved nonisothermal cooling, with an initial metal temperature of 2000 °C and a lower initial fiber temperature of 20, 500, and 1000 °C. A cooling rate was imposed on the metal, simulating cooling of the droplet from heat exchange with the surroundings, and thermal gradients forming in the fiber by conduction. Two cooling rates were investigated. Two external boundary conditions were set for the fiber: adiabatic (i.e., no heat loss to the surroundings) or with an imposed external temperature of 20 °C, representing the limiting cases of thermal transfer with the surroundings.

4.2 Results and Discussion

All calculations show that the two points that experienced the highest stresses are the points called "axe" and "lim" (for the axis and border), as shown in Fig. 8. Table 3 summarizes the values of the highest stresses, their location, and the time at which they are reached for each calculation.

It is seen that stresses arising purely from CTE differences were not very high. For nonisothermal calculations, however, strong temperature gradients are established at the beginning and reduce with time. Very high stresses may therefore develop, which reach their peak value during cooling when the temperature gradients are still steep. Their value can go up to almost 2 GPa of tensile stress at the axis point, close to the experimental value of coating damage measured earlier by Gagnot (Ref 10). These stress values should only be considered as indications because the material parameters and boundary conditions were only estimations. They could, however, indicate trends to minimize fiber damage. Heating the fibers, as expected, would reduce the thermally induced stresses. Another way would be to reduce the cooling rate. This would be rather difficult to obtain practically because metal cooling is governed by heat transfer with the surroundings in the plasma chamber.

5. Lattice-Gas Modeling of Droplet Deposition

The quality of coatings obtained by plasma deposition of layers depends on many factors, including the formation of defects (unmelted particles and porosity) during this complex process. To study coating buildup and resulting microstructures, a probabilistic model at a microscopic scale for droplet deposition onto a substrate was proposed. This model could simulate plasma spraying onto a rough substrate and was implemented in software operating in two dimensions (Ref 7, 15). For application to TMCs, the substrate roughness arises from the array of fibers. This approach differs from other models based on a thermal or thermomechanical approach (Ref 16, 17), which does not involve the flow of liquid droplets against a solid obstacle, as required in plasma spraying.

5.1 Fundamentals of LGM

Lattice-gas modeling involves the representation of particles moving and interacting on a graph. Formerly developed by physicists to simulate the hydrodynamics of complex flows (Ref 18-20), LGM can be used to simulate random structure generation on a physical basis (Ref 21). The basic model uses rules of conservation involved in collisions of particles and boundary conditions. First applications were to simulate complex flows in random porous media (Ref 22, 23). This led to estimation of the permeability and properties of dispersion of fluids as a function of microgeometry. By addition of aggregation rules, it was possible to generate random aggregates and to study simulation processes involving nucleation and growth phenomena in a changing velocity field (Ref 24-26). When involving forces of attraction or repulsion between various species, immiscible fluid flows (Ref 27, 28) and phase separations (such as liquid-gas in Ref 29) could be simulated.

5.2 Simulation of Thermal Spray Coating Buildup

A lattice-gas model for deposition of droplets onto a substrate was developed to simulate plasma layer deposition onto a rough substrate. This approach can reproduce various conditions of deposition and generates, at the scale of hundreds of micrometers to millimeters, random coatings with a complex geometry from a population of droplets.

The first step of the model generates stable droplets in a surrounding medium, namely a carrier gas. This is obtained from a two-species model, the immiscible lattice gas, which generates a surface tension ensuring stable droplets with a radius larger than 10 pixels. The second step simulates the deformation of droplets when impinging on a substrate. The motion of droplets is generated by random deflection of every gas particle in the direction of motion. Edge effects on obstacles are avoided by letting them be transparent to the carrier gas, while the solid cores contained in the droplets are bounced back. It was shown from simulations that a correct sequence of droplet deposition could be reproduced, with the generation of a shock wave during the contact with the substrate. The last step reproduces the rapid solidification of a droplet during impact on the substrate. This is implemented during the contact with the particles of the droplet being able to aggregate randomly on the solid (the initial substrate or the layer during its evolution). The coating process was simulated by the introduction of a sequence of droplets.

The main parameters of the model to generate simulations are the number of simulation steps (resulting in various coating thickness), the size of the system (i.e., the coating length), the size distribution and the angle of incidence of droplets, the probabilistic distribution of the aggregation probability, and the initial topography of the substrate. A heterogeneous temperature distribution for the droplets can be involved, which can reproduce the generation of defects in the coating.

Simulating the thermal spray coating by means of the LGM approach will help in establishing a connection between the plasma operating conditions (namely the inflight particles properties), coating microstructure, and coating properties as might be predicted by finite element modeling. Changing the input parameters of the simulations can provide guidelines to prevent coatings from defects and to design optimal coatings for given

physical (mainly thermoelastic) properties. For a given experimental system, the effect of input parameters of the LGM software could be investigated, that is, rheology and temperature distribution of the melted particles, size distribution of droplets, conditions of solidification on the substrate, and roughness of the substrate. This is illustrated in Fig. 9, where the temperature of a droplet is given by the probability of aggregation of its gas particles to the substrate (and to already aggregated particles), P_a, resulting in different shapes (and different times, t) for the solidification process.

In Fig. 10, a sequence of droplets were deposited onto a fiber array. In practical applications, for given operating conditions (type of substrate and droplets), the model has to be calibrated using an adequate choice of parameters, such as the probability of aggregation and statistical distribution, the viscosity of the fluid, the size distribution of droplets, and the initial roughness of the substrates. For this step, the LGM approach must be validated from data. For a given set of experimental conditions, this can be carried out by means of comparisons between simulated and actual sequences of deposition and by means of comparative image analysis of layers obtained by experiments and by simulations.

6. Conclusions

This study presents the development of three tools to help achieve high-quality TMCs, that is, (1) controlling the cleanliness of the sprayed material, (2) controlling fiber damage, and (3) examining the coating buildup.

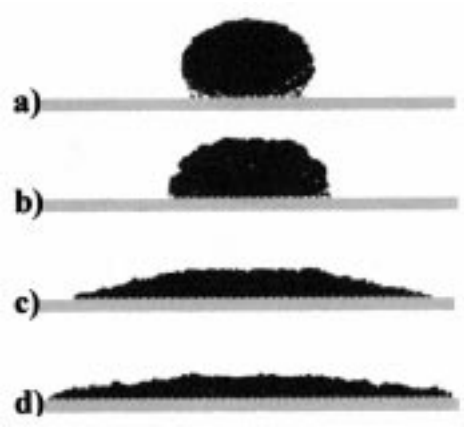

Fig. 9 Effect of the aggregation probability, P_a, on the droplet morphology given by LGM at the end of deposition. (a) $P_a = 0.8$, $t = 350$. (b) $P_a = 0.15$, $t = 450$. (c) $P_a = 0.02$, $t = 1000$. (d) $P_a = 0.01$, $t = 1300$ (time, t, in an arbitrary unit)

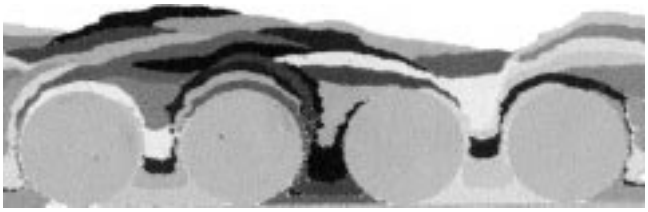

Fig. 10 Lattice-gas modeling simulation of coating buildup onto fibers (t = 50,000, 33 droplets)

First, a thorough analysis of oxygen contamination was shown to be feasible using EPMA of elementary particles. This led to an interpretation involving diffusion phenomena. Second, thermomechanical modeling using finite element analysis allowed for an estimation of fiber damage at the spraying stage. This resulted in specifications for a processing route to improve the material. The third part of the work exhibited a new model of deposition based on lattice-gas concepts. The potential of this type of model was shown to be high for application to composites. This is an industry-friendly model because the results can be quickly and easily displayed and may involve a large range of spraying and material conditions.

Acknowledgment

This work was supported by DRET under contract No. 92.017.00.022. Mrs N. De Dave, Dr. V. Guipont, and Mr. F. N'Guyen of the Ecole des Mines de Paris are also gratefully acknowledged for technical assistance, fruitful discussions, and help in confocal microscopy.

References

1. P.A. Siemers, "Method for Continuous Fabrication of Fiber Reinforced Titanium-Based Composites," EU Patent 0 358 801 A1, 21 March 1990
2. P.A. Siemers, "RF Plasma Method of Forming Multilayer Reinforced Composites," EU Patent 0 358 804 A1, 21 March 1990
3. J. Kumpfert, R. Leucht, J. Hemptenmacher, and H.J. Dudek, Effects of Matrix Properties on TMC Properties, *Proc. of ECCM-7*, Vol 1, (London, UK), 14-16 May 1996, Institute of Materials, London, UK, 1996, p 419-425
4. R.R. Kieschke and T.W. Clyne, Interfacial Bond Strength between SiC Monofilaments and Spray-Deposited Titanium, *Proc. of ICCM7*, Vol 2, Pergamon Press, Oxford, UK, 1990, p149-158
5. R.R. Kieschke and T.W. Clyne, Pull-Out Testing of SiC Monofilaments in a Spray-Deposited Ti Matrix, *Interfacial Phenomena in Composite Materials*, Butterworths, London, UK, 1989, p 282-293
6. T.W. Clyne and K.A. Robert, The Influence of Process Parameters on Consolidation Efficiency when Forming Composites by Spraying onto Monofilaments, *Acta Metall. Mater.*, Vol 43, 1995, p 2541-2550
7. E. Cochelin, F. Borit, L. Decker, D. Jeulin, V. Guipont, and M. Jeandin, Application of Lattice-Gas Modeling to Plasma Spraying, *Proc. 11th Int. Conf. Surface Modification Technologies (SMT11)* (Paris, France) 8-11 Sept 1997, Institute of Materials, London, UK, 1997, p 21-30
8. H. Gruner and A.R. Nicoll, Process Quality Control during Vacuum Plasma Spraying with Oxygen Sensitive Materials, *Corrosion 1984*, Institute of Corrosion Science & Technology, London, UK, 1984, p 29-35
9. K.A. Roberts and T.W. Clyne, A Simple Procedure for the Characterization of Spray Deposition Processes—The Linescan Test, *Surf. Coat. Technol.*, Vol 41, 1990, p 103-115
10. D. Gagnot, "Evaluation des Différents Contributeurs à l'Endommagement des Fibres Longues en Projection Plasma" ("Study of the Main Parameters Influencing Long Fiber Damage in Plasma-Sprayed Composites"), Internal Report, Matra-Défense/Ecole des Mines de Paris, June 1993 (in French)
11. S. Ochiai, K. Osamura, and K. Honjo, Influence of Fracture of Coating Layer on Fiber Strength, *Mater. Sci. Eng.*, Vol A154, 1992, p 149-154
12. M. Rolland, "Spray Forming, Droplet Microstructure and Impingement Behavior," M.S. thesis, MIT, Cambridge, MA, Feb 1996
13. W.F. Smith, *Structure and Properties of Engineering Alloys*, McGraw-Hill, 1981
14. *Metals Handbook*, Desk Edition, American Society for Metals, 1985, p 1.50-1.52 and p 9.11

15. L. Decker and D. Jeulin, Random Texture Simulation by Multi-Species Lattice Gas Models, *J. Electron. Imaging*, Vol 6, 1997, p 78-93
16. H. Fukanuma, Mathematical Modeling of Flattening Process on Rough Surfaces in Thermal Spray, *Proc. Ninth National Thermal Spray Conference*, (Cincinnati, OH), 7-11 Oct 1996, ASM International, 1996, p 647-656
17. G. Jaccuci, S. Cirolini, M. Marchese, and J.H. Harding, Computer Modeling of the Manufacturing Process of Ceramic Thermal Barrier Coatings, *Proc. Third Int. Conf. Computational Plasticity*, (Barcelona, Spain) 6-10 April 1992, Pineridge Pres Ltd., 1992, p 1683-1695
18. J. Hardy, O. De Pazzis, and Y. Pomeau, Molecular Dynamics of a Classical Lattice Gas: Transport Properties and Time Correlation Functions, *Phys. Rev. Lett.*, Vol A13, 1976, p 1949-1961
19. U. Frisch, B. Hasslacher, and Y. Pomeau, Lattice-Gas Automata for the Navier-Stokes Equation, *Phys Rev. Lett.*, Vol 56, 1986, p 1505-1508
20. U. Frisch, D. D'Humières, B. Hasslacher, P. Lallemand, Y. Pomeau, and J.P. Rivet, Lattice Gas Hydrodynamics in Two and Three Dimensions, *Complex Systems*, Vol 1, 1987, p 649-707
21. D. Jeulin, Random Structures Generation by Lattice Gas, *Acta Stereol.*, Vol 15, 1996, p 31-43
22. D.H. Rothman, Cellular Automaton Fluids: A Model for Flow in Porous Media, *Geophysics*, Vol 53, 1988, p 509-518
23. D. Jeulin, Flow and Diffusion in Random Porous Media, *Numerical Methods for the Simulation of Multiphase and Complex Flow*, Springer-Verlag, Berlin, Germany, 1992, p 106-123
24. R. Brémond and D. Jeulin, Random Media and Lattice Gas Simulations, *Geostatistical Simulations Workshop*, Kluwer Academic, Dordrecht, Netherlands, 1994, p 89-105
25. R. Brémond and D. Jeulin, Morphogenesis Simulations with Lattice Gas, *Mathematical Morphology and Its Applications to Image Processing*, Kluwer Academic, Dordrecht, Netherlands 1994, p 297-304
26. R. Brémond, D. Jeulin, and M. Abouaf, Simulation of the Filtration of Cast-Iron, *Rev. Mét. CIT/Science et Génie des Matériaux*, Vol 5, 1995, p 593-606 (in English and French)
27. D.H. Rothman, Macroscopic Laws for Immiscible Two-Phase Flow in Porous Media: Results from Numerical Experiments, *J. Geophysic. Res.*, Vol 95, 1990, p 8663-8674
28. D.H. Rothman and J.M. Keller, Immiscible Cellular-Automaton Fluids, J. Statistic. Phys., Vol 52, 1998, p 1119-1127
29. C. Appert , D.H. Rothman, and S. Zaleski, A Liquid-Gas Model on a Lattice, *Phys. D*, Vol 47, 1991, p 85-96